Pyridylphenyl appended imidazoquinazoline based ratiometric fluorescence ‘‘*turn-on’’* chemosensor for Hg^{2+} and Al^{3+} in aqueous media

Amit Kumar, Rampal Pandey, Ashish Kumar, and Daya Shankar Pandey*

Department of Chemistry, Faculty of Science, Banaras Hindu University, Varanasi - 221 005, India

Supporting Information Placeholder

Contents:

Experimental section

Materials and methods

The common reagents and solvents were acquired from Merck, Qualigens and S. D. Fine Chem. Ltd, Mumbai. Solvents were dried and distilled following the standard procedures prior to their use.[1] 4-(pyridin-4-yl)benzaldehyde, 2-aminophenylbenzimidazole and metal nitrates *viz.*, $NaNO_3$, KNO_3, $Ca(NO_3)_2{\cdot}4H_2O$, $Mg(NO_3)_2{\cdot}6H_2O$, $Al(NO_3)_2{\cdot}9H_2O$, $Fe(NO_3)_3{\cdot}9H_2O$, $Co(NO_3)_2{\cdot}6H_2O$, $Ni(NO_3)_2{\cdot}6H_2O$, $Cu(NO_3)_2{\cdot}3H_2O$, $Zn(NO_3)_2{\cdot}6H_2O$, $Cd(NO_3)_2{\cdot}4H_2O$, $AgNO_3$, $Pb(NO_3)_2$ and $Hg(NO_3)_2{\cdot}H_2O$ were obtained from commercial sources and used without further purifications.

Elemental analyses for C, H and N were performed on a CE-440 Elemental Analyzer. Infrared and electronic absorption spectra were obtained on a Perkin-Elmer Spectrum Version 10.03.05 FT-IR and Shimadzu UV-1601 spectrophotometers, respectively. ^{1}H (300 MHz) and ^{13}C (75.45 MHz) NMR spectra were obtained on a JEOL AL300 FT-NMR spectrometer using tetramethylsilane ($Si(CH_3)_4$) as an internal reference. Fluorescence spectra were recorded on a PerkinElmer LS 55, Fluorescence Spectrometer (U.K.). Electrospray ionization mass spectrometric (ESI-MS) data were obtained on a JEOL Accu TOF JMS-T100 LC mass spectrometer.

Synthesis of 6-(4-(pyridin-4-yl)phenyl)-5,6-dihydrobenzo[4,5]imidazo[1,2-c]quinazoline (1)

An ethanolic solution of 4-(pyridin-4-yl)benzaldehyde (2.0 mmol, 10 mL) was added to a stirring solution of 2-(2-aminophenyl)-1-benzimidazole (2.0 mmol) dissolved in the same solvent (20 mL) and the contents of the flask was heated under reflux for 10 h. After cooling to ambient temperature, it was concentrated at reduced pressure to half its volume and kept undisturbed at rt. The microcrystalline compound thus obtained was separated by filtration, washed with cold ethanol followed by diethylether. Yield (0.605 g, 81%). Analytical data: calcd. $C_{25}H_{18}N_4$ (374.43): C, 80.19; H, 4.85; N, 14.96, Found: C, 80.09; H, 4.76; N, 14.85. FT-IR (KBr; cm^{-1}): 3219 (m), 1612 (s), 1597 (vs), 1533 (m), 1504 (vs), 1474 (vs), 1447 (m), 1405 (m), 1384 (s), 1320 (w), 1284 (vs), 1257 (m), 807 (s), 751 (s), 733 (vs). ^{1}H NMR (DMSO-d_6, 300 MHz, δ_H, ppm): 8.57 (d, 2*H*); 7.97 (d, 1*H*); 7.72-7.59 (m, 2H); 7.35-7.11 (m, 6*H*); 6.87–6.80 (m, 2*H*). ^{13}C NMR (DMSO-d_6, 75 MHz, δ_C, ppm): 150.1, 146.8, 146.2,

143.8, 142.9, 141.4, 137.6, 132.8, 131.7, 127.3, 126.5, 124.6, 122.3, 122.1, 121.1, 118.7, 114.9, 111.80, 110.4, 67.1. HRMS (*m/z*): 375.1603 (calcd 375.1610); $[M+H]^+$.

Absorption and Emission Studies

Stock solution of **1** for the electronic absorption/emission studies was prepared in EtOH/H_2O (1:99, v/v; *c*, 10 μM). The solution of various metal ions (Na^+, K^+, Mg^{2+}, Ca^{2+}, Al^{3+}, Fe^{3+}, Co^{2+}, Ni^{2+}, Cu^{2+}, Zn^{2+}, Cd^{2+}, Hg^{2+}, Ag^+ and Pb^{2+}) were prepared by dissolving their nitrate salts in triple distilled (TD) water (c; 10 mM). For the titration experiments 3.0 mL solution of **1** (10 μM) was taken in a quartz cuvette (path length 1 cm) and solution of the metal ions were gradually added with the help of a micro pipette. In titration experiments time interval was maintained as 2 minute for addition of each fraction of metal ions to make a complete reaction between **1** and analytes.

Calculation of limit of detection (LOD)

Quantitative responses of **1** toward Hg^{2+} and Al^{3+} were investigated using linear calibration plots from fluorescence spectral studies. Dynamic range for determination of LOD for these ions has been found to be linear. The LOD has been evaluated using $3\sigma/s$, where σ is the standard deviation of the blank signals and *s* is the slope of the linear calibration plot.

Theoretical Calculation

Molecular structure of **1**, **1**+Hg^{2+} and **1**+Al^{3+} were designed using ChemBioDraw Ultra software and 3D views of these structures were optimized by minimizing energy of the molecule using MM2 mode in the same software. The optimization and energy calculations for these were performed on Gaussian09 with a density functional theory (DFT) in the B3LYP mode in the ground state.[2-3] The basis set 6-31G(d,p) has been used for all the light atoms (C, H , N, O) while LANL2DZ for the metal atoms (Al, Hg) with an effective-core pseudo-potential.[4]

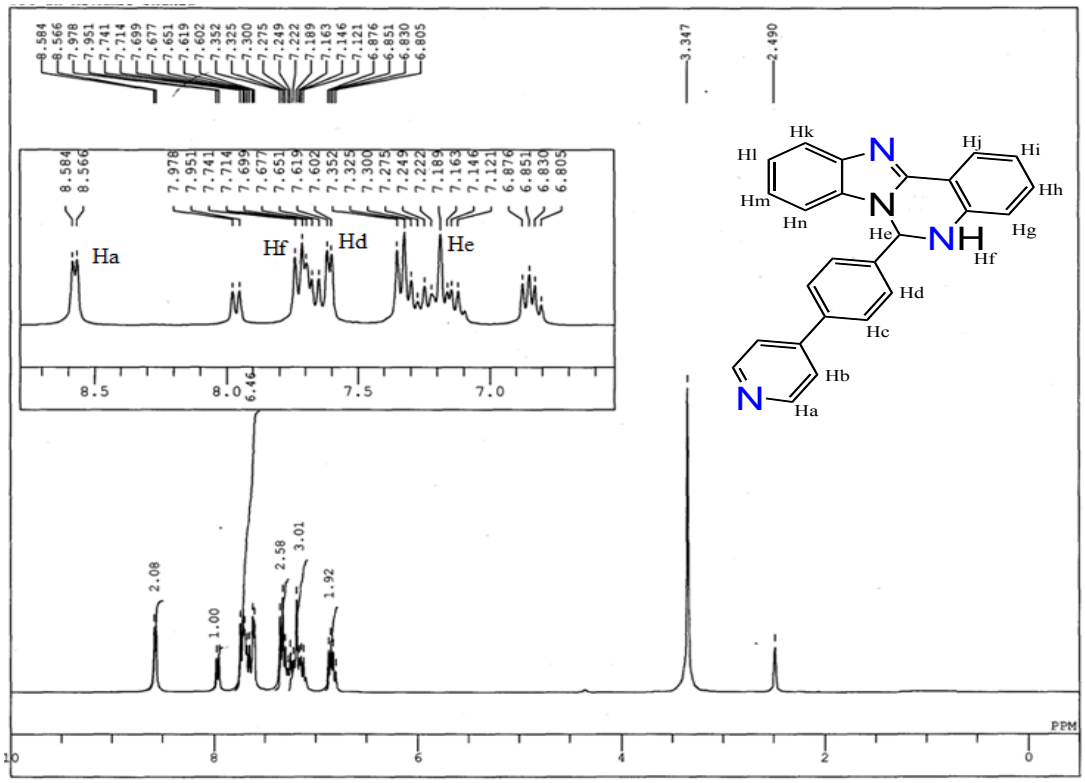

Fig. S1 ^{1}H NMR spectrum with labelling of some characteristic protons of **1**.

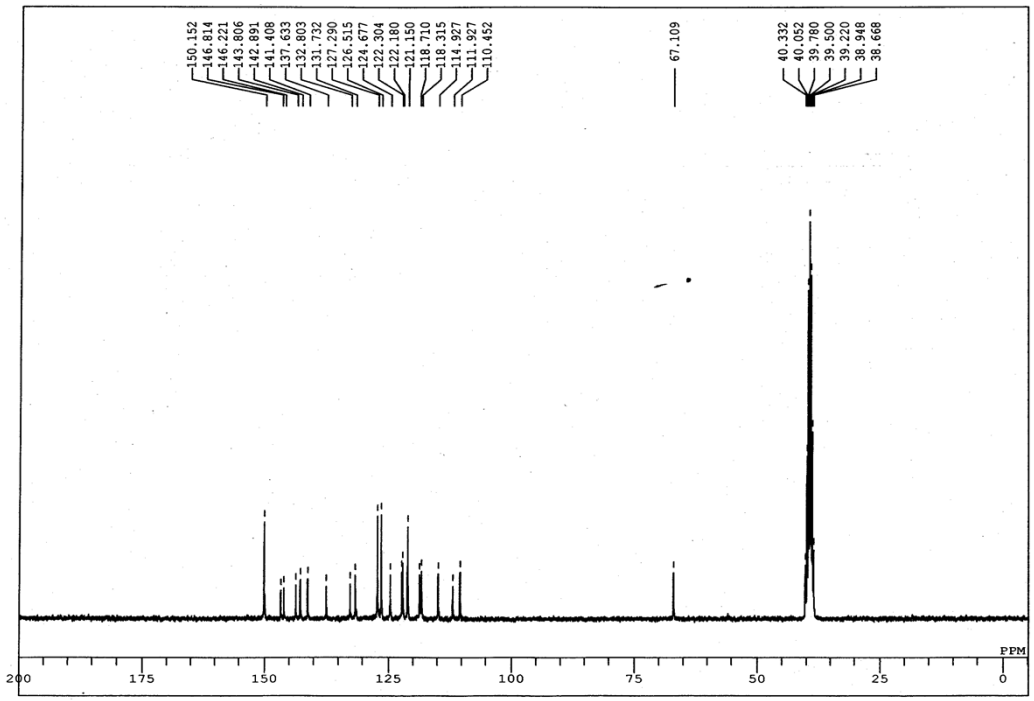

Fig. S2 ^{13}C NMR spectrum of **1**.

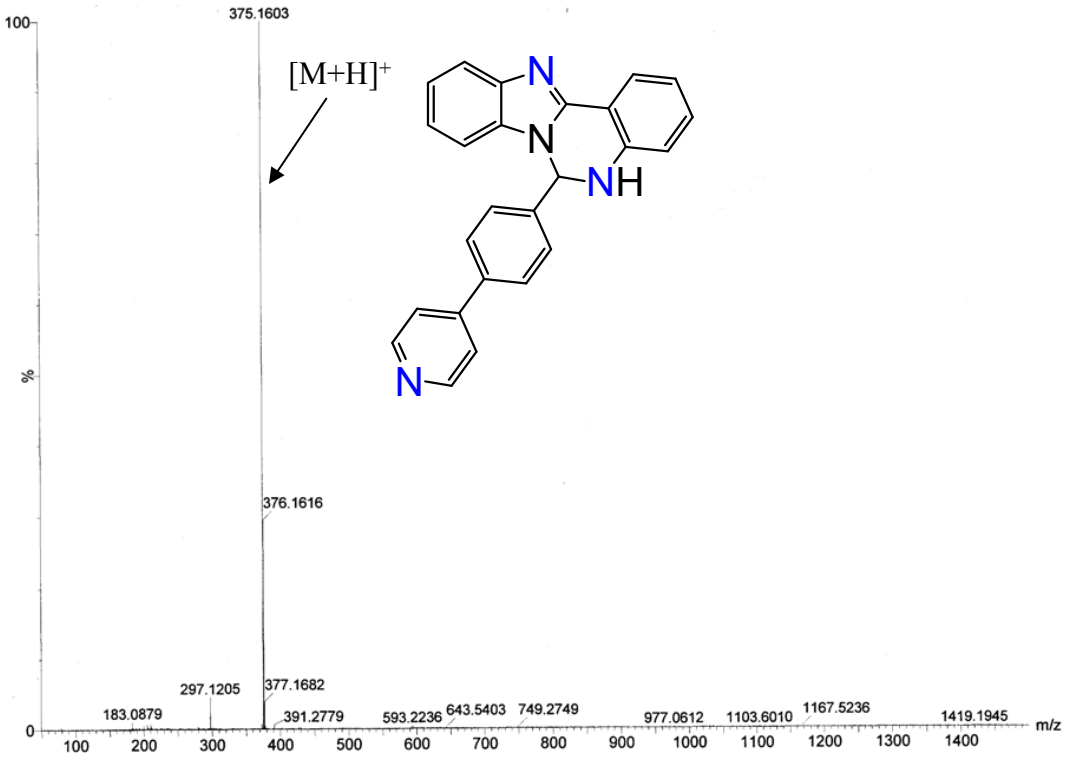

Fig. S3 ESI-Mass spectrum of **1**.

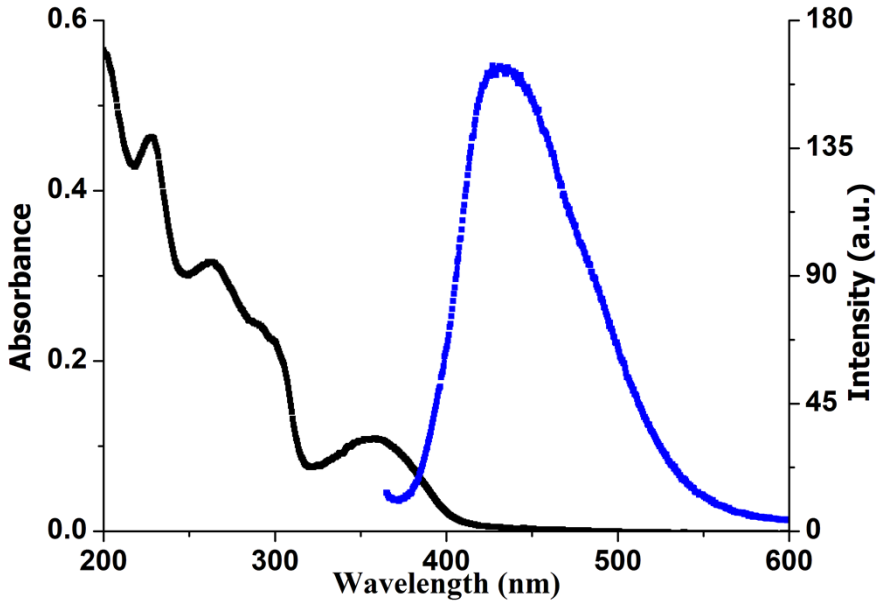

Fig. S4 UV/vis and fluorescence spectra of **1**.

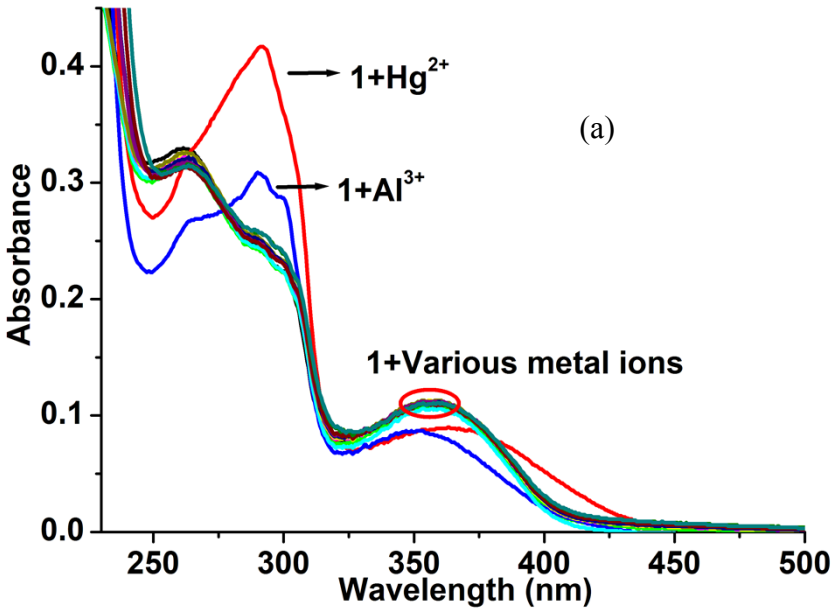

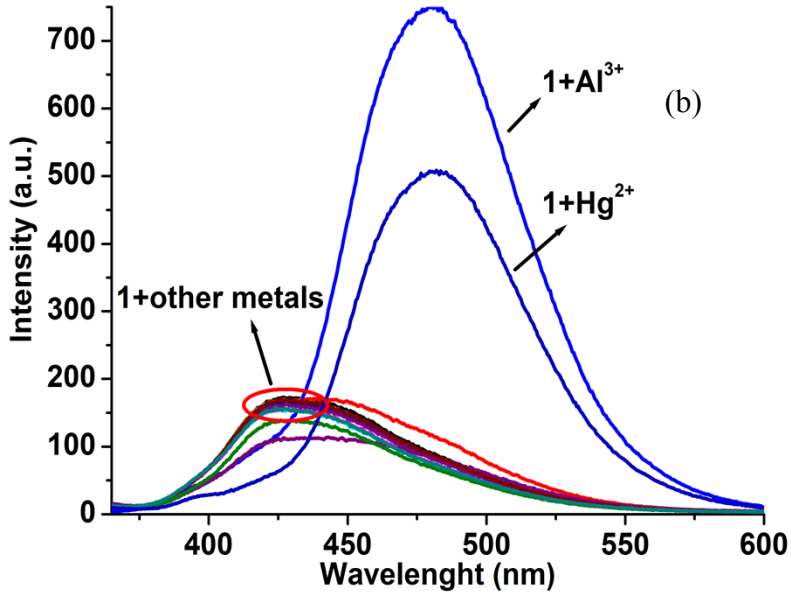

Fig. S5 UV/vis (a) and fluorescence (b) spectral changes for **1** in presence of 10 equiv. of various metal ions *viz.,* Na^{+}, K^{+}, Mg^{2+}, Ca^{2+}, Al^{3+}, Fe^{3+}, Co^{2+}, Ni^{2+}, Cu^{2+}, Zn^{2+}, Cd^{2+}, Hg^{2+}, Ag^{+} and Pb^{2+}.

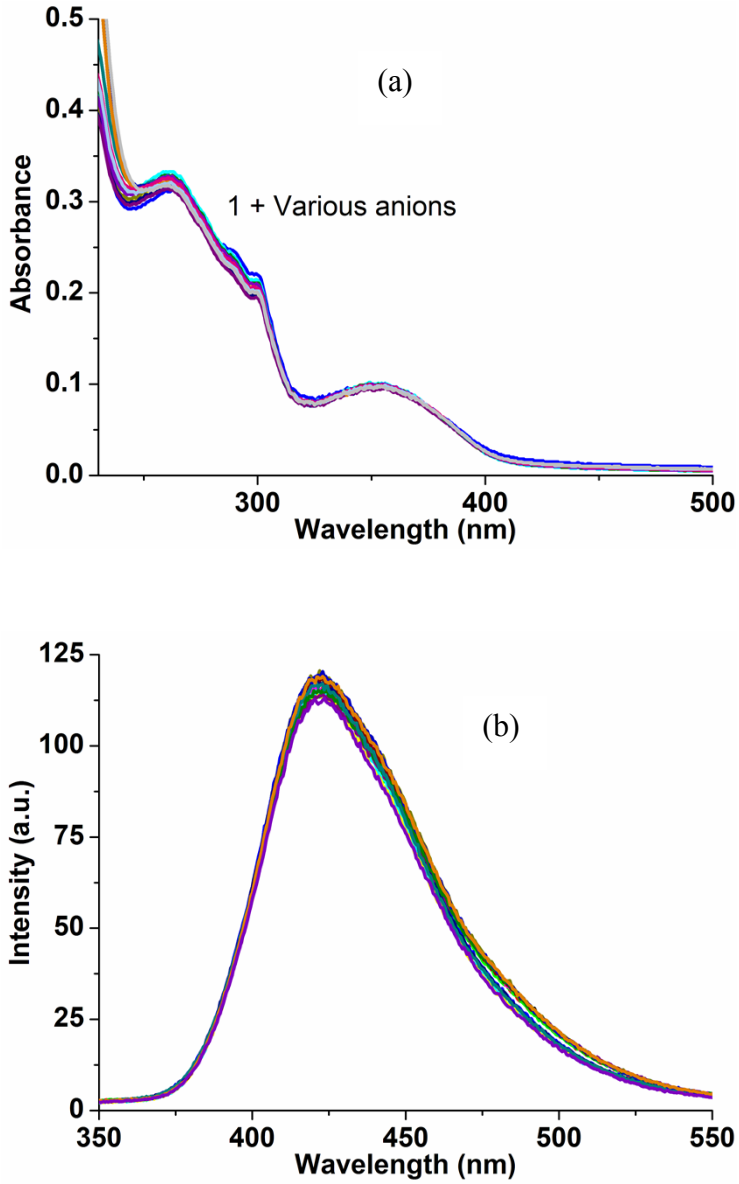

Fig. S6 UV/vis (a) and fluorescence (b) spectral changes for **1** in presence of 10 equiv. of various anions *viz.* F^-, Cl^-, Br^-, I^-, $SO4^{2-}$, S^{2-}, HSO_4^-, SO_3^{2-}, $S_2O_3^{2-}$, $S_2O_8^{2-}$, CO_3^{2-}, NO_2^-, NO_3^- and PO_4^{3-}.

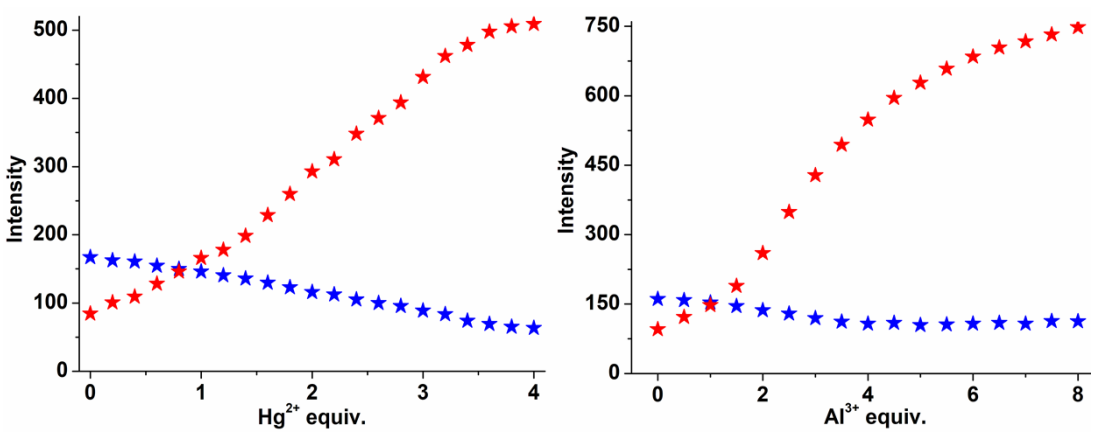

(a) (b)

Fig. S7 Ratiometric fluorescence response of **1** at 425 nm (blue star showing quenching behaviour), and 482 nm (red star showing enhancement) with the addition of Hg^{2+} (a) and Al^{3+} ions (b).

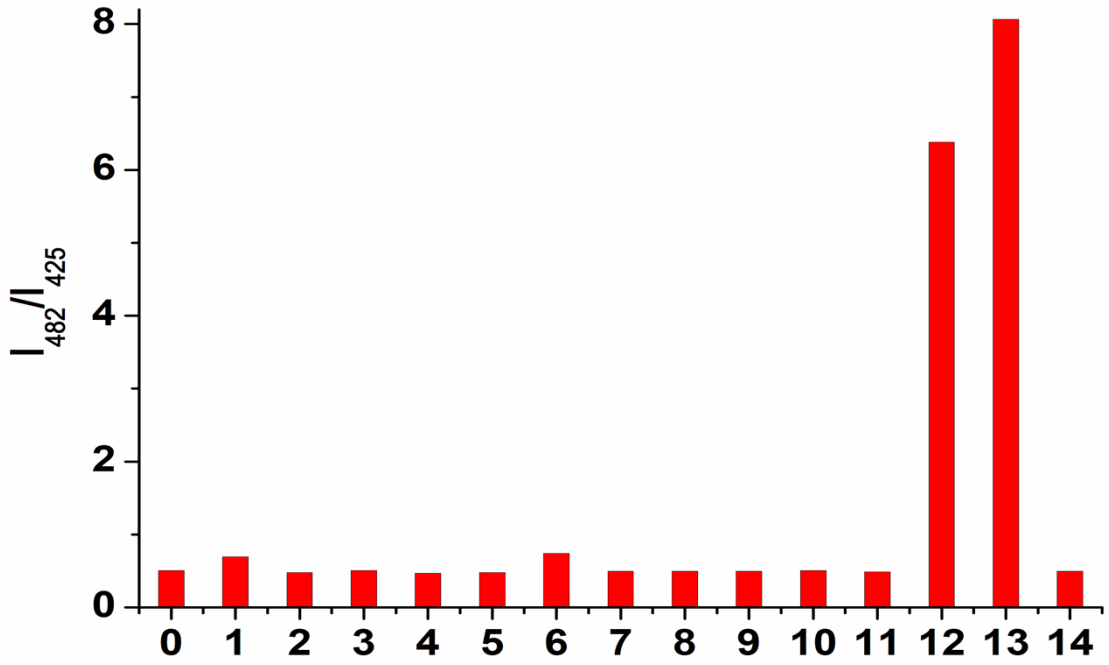

Fig. S8 Bar diagram showing the fluorescence intensity ratio (I_{482}/I_{425}) for **1** in absence (0) and presence of various metal ions *viz.,* [Na^{+}, (1); K^{+}, (2); Mg^{2+}, (3); Ca^{2+}, (4); Fe^{3+}, (5); Co^{2+}, (6); Ni^{2+}, (7); Cu^{2+}, (8); Zn^{2+}, (9); Cd^{2+}, (10); Ag^{+}, (11); Al^{3+}, (12); Hg^{2+}, (13) and Pb^{2+}, (14)].

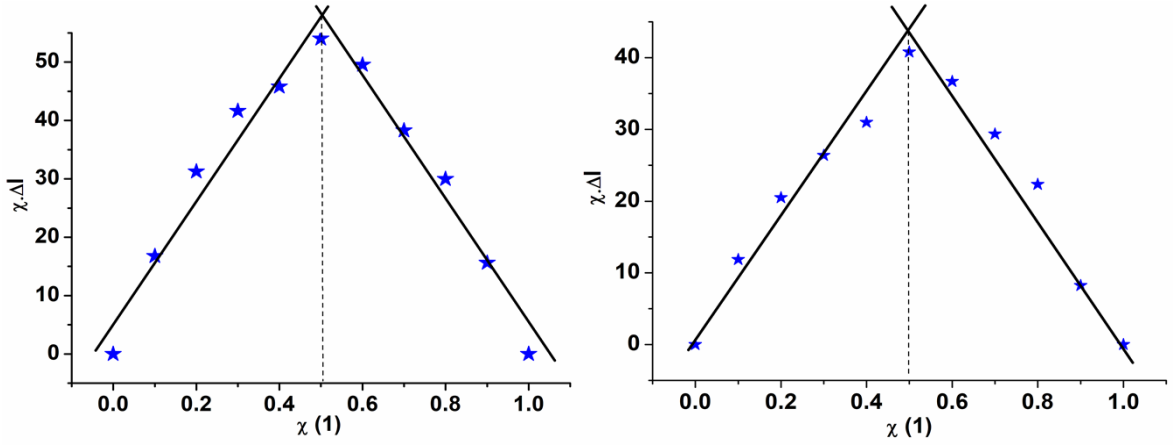

(a) (b)

Fig. S9 Job's plot analysis illustrating 1:1 stoichiometry for complex **1** with Hg^{2+} (a) and Al^{3+} (b) by the fluorescence spectra.

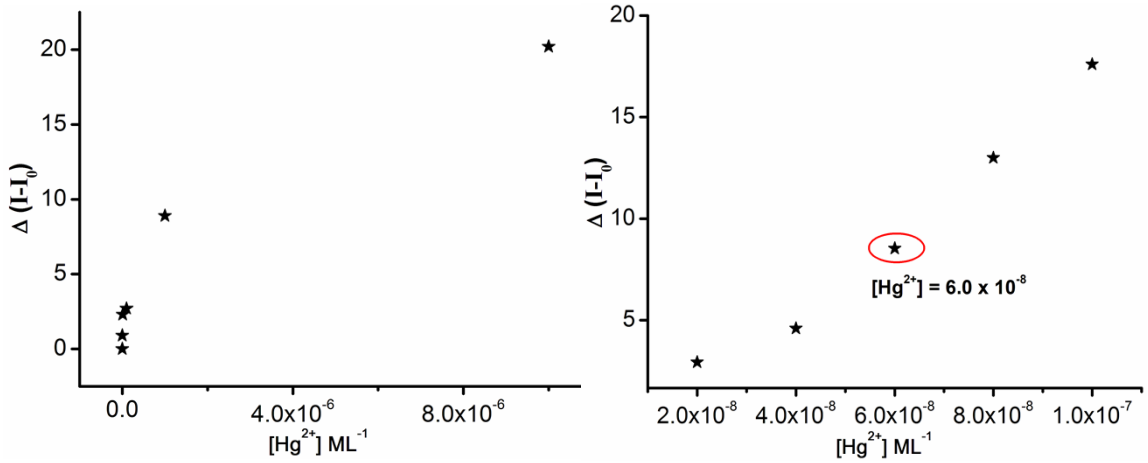

(a) (b)

Fig. S10 Plot of $\Delta(I\text{-}I_0)$ *vs.* $[Hg^{2+}]$ with [**1**] = 10 μM for the calculation of lowest detection limit: plot for varying $[Hg^{2+}]$ of 0.0-1.0×10^{-5} M, (a); and same plot to show the lower concentration for Hg^{2+} which shows the linear part of the plot and is used for determining the lowest detectable concentration of Hg^{2+} (6.0×10^{-8}) (b); and the LOD for Hg^{2+} has been calculated by standard analytical method using equation $3\sigma/s$ and found to be 1.69×10^{-8} M.

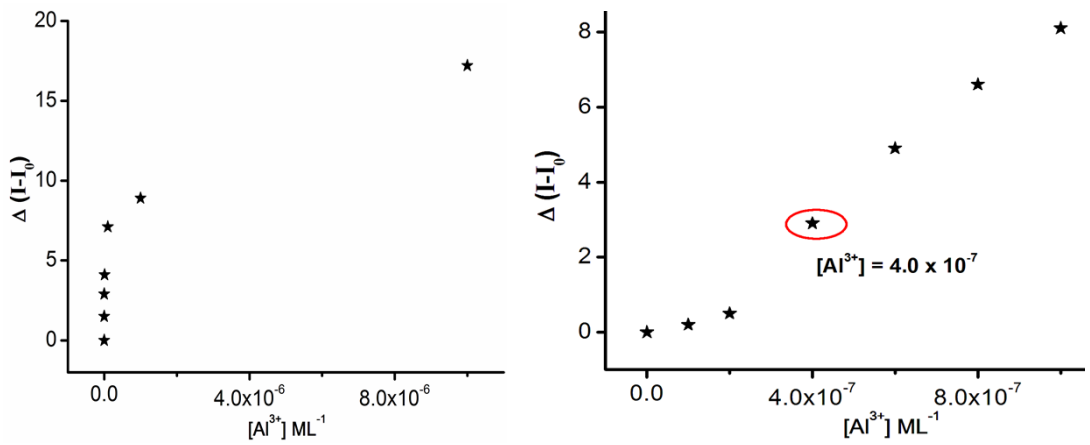

(a) (b)

Fig. S11 Plot of $\Delta(I\text{-}I_0)$ *vs.* $[Al^{3+}]$ with [**1**] = 10 μM for the calculation of lowest detection limit: plot for varying $[Al^{3+}]$ of 0.0-1.0×10^{-5} M, (a); and same plot to show the lower concentration for Al^{3+} which shows the linear part of the plot and is used for determining the lowest detectable concentration of Al^{3+} (4.0×10^{-7}) (b); and the LOD for Al^{3+} has been calculated by standard analytical method using equation $3\sigma/s$ and found to be 1.44×10^{-7} M.

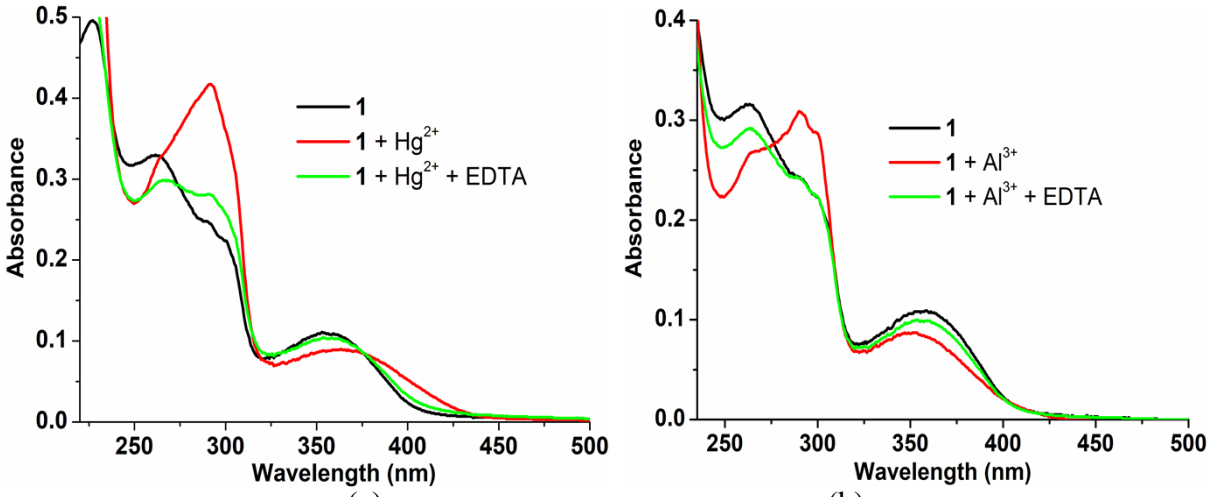

(a) (b)

Fig. S12 Reversibility and reusability of the probe **1** showing by absorption spectra of **1** + Hg^{2+} (a), and **1** + Al^{3+} (b) in presence and absence of EDTA (~10.0 equiv).

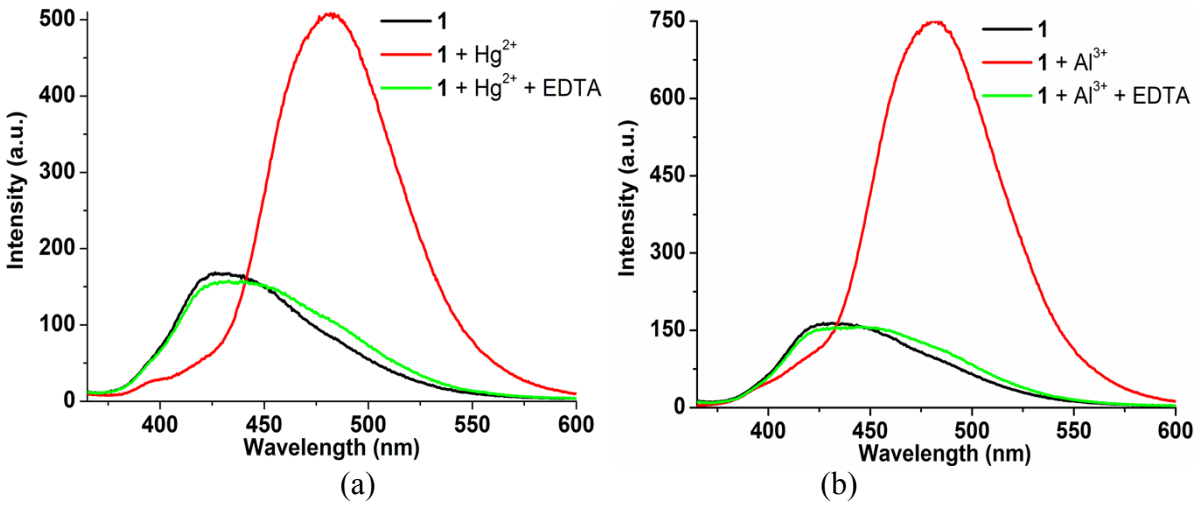

Fig. S13 Reversibility and reusability of the probe **1** showing by emission spectra of **1** + Hg^{2+} (a) and **1** + Al^{3+} (b) in presence and absence of EDTA (~10.0 equiv).

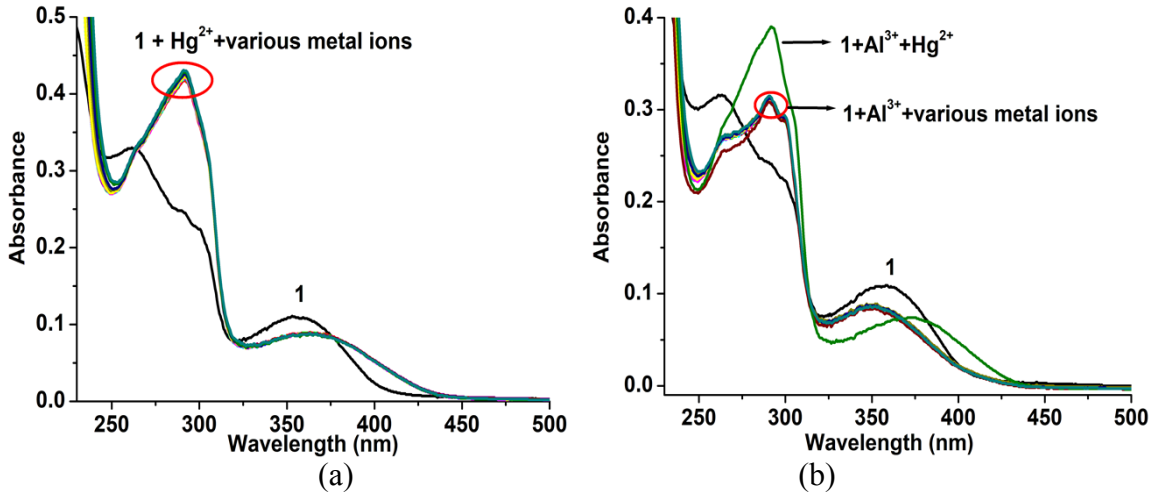

Fig. S14 UV/vis spectral changes for **1** with Hg^{2+} (a) and Al^{3+} (b) in presence of the interference of various metal ions *viz.,* Na^{+}, K^{+}, Mg^{2+}, Ca^{2+}, Al^{3+}, Fe^{3+}, Co^{2+}, Ni^{2+}, Cu^{2+}, Zn^{2+}, Cd^{2+}, Ag^{+} and Pb^{2+}.

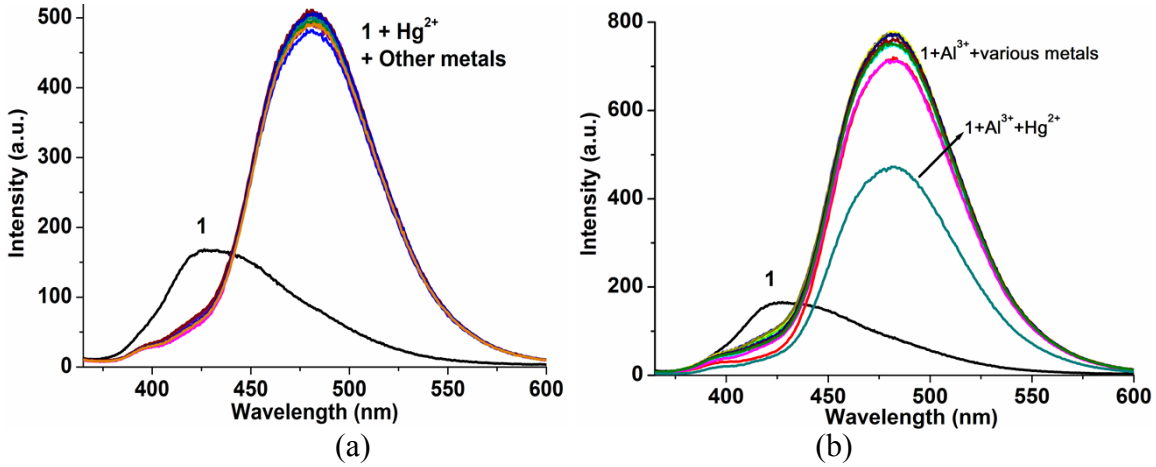

Fig. S15 Fluorescence spectral changes for **1**·Hg^{2+} (a) and **1**·Al^{3+} (b) in presence of the interference of various metal ions *viz.,* Na^{+}, K^{+}, Mg^{2+}, Ca^{2+}, Al^{3+}, Fe^{3+}, Co^{2+}, Ni^{2+}, Cu^{2+}, Zn^{2+}, Cd^{2+}, Ag^{+} and Pb^{2+}.

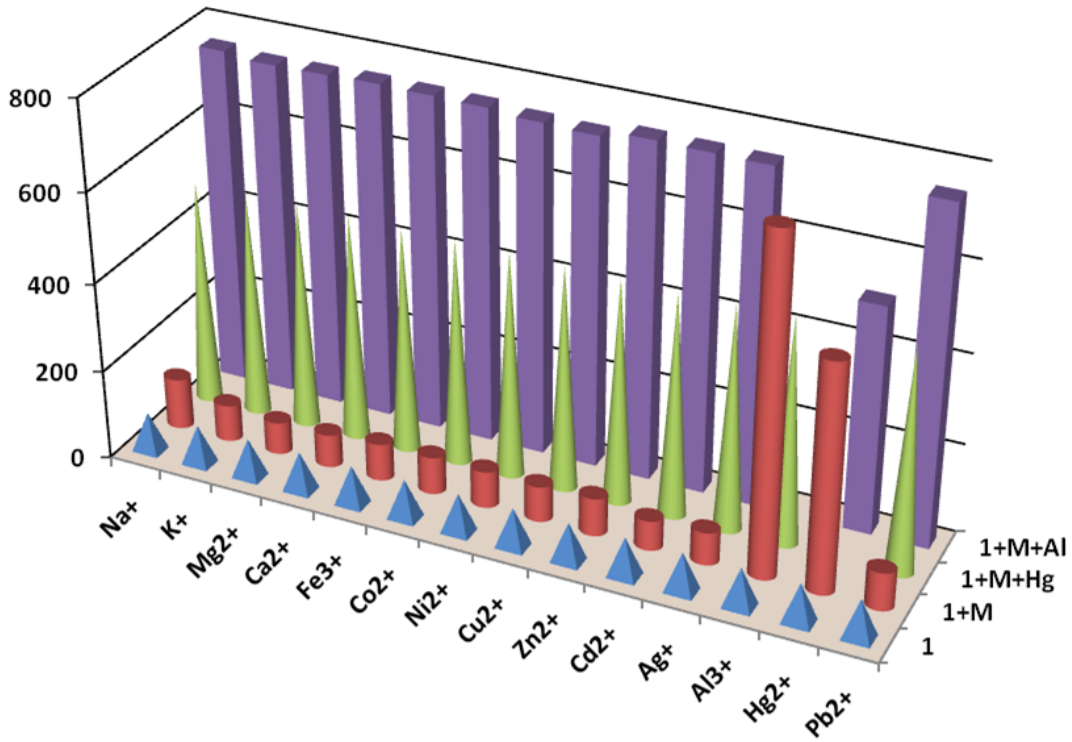

Fig. S16 Bar diagram showing the fluorescence spectral changes at 482 nm for **1** with Hg^{2+} and Al^{3+} in presence of the interference of various metal ions *viz.,* Na^{+}, K^{+}, Mg^{2+}, Ca^{2+}, Al^{3+}, Fe^{3+}, Co^{2+}, Ni^{2+}, Cu^{2+}, Zn^{2+}, Cd^{2+}, Ag^{+} and Pb^{2+}; [blue pyramid, **1**; red cylinder, **1** + various metal ions; green cone, **1** + Hg^{2+} + other metal ions and purple rod, **1** + Al^{3+} + other metal ions].

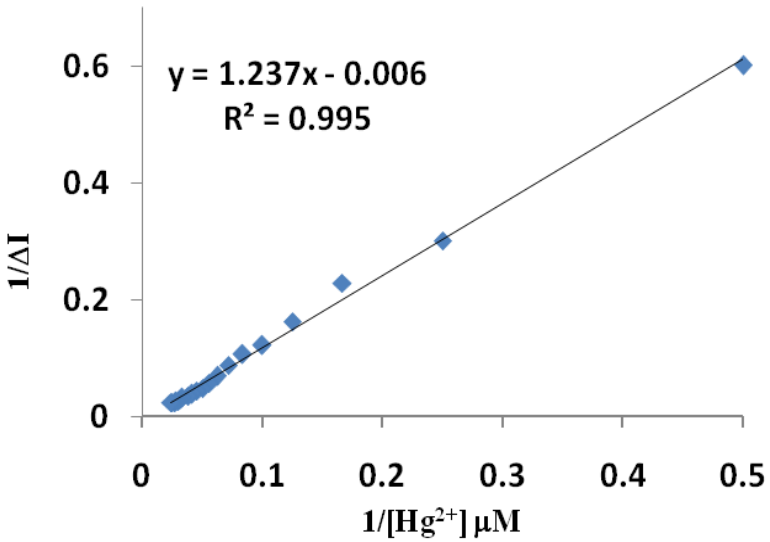

Fig. S17 Benesi−Hildebrand plot for PPC and Hg^{2+} to calculate the binding constant (K_a=4.12 × 10^4).

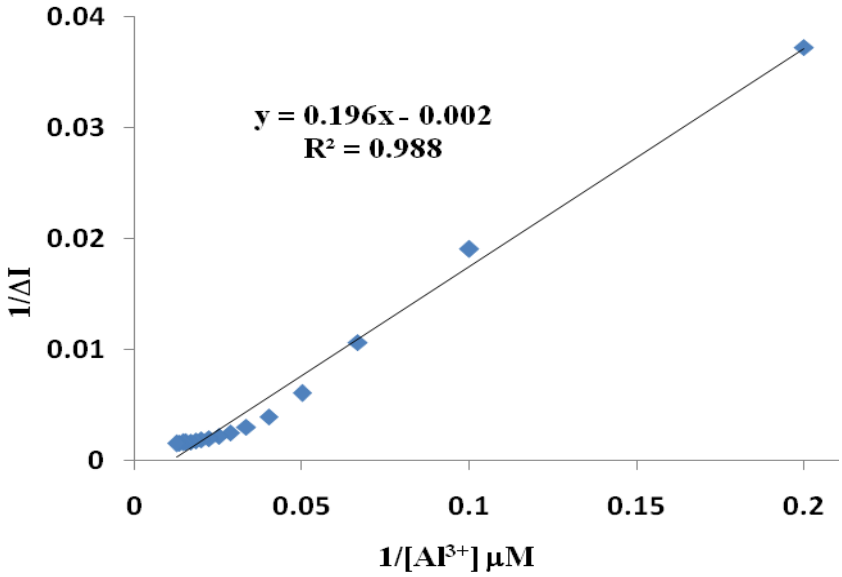

Fig. S18 Benesi−Hildebrand plot for PPC and Al^{3+} to calculate the binding constant (K_a=2.45 × 10^3).

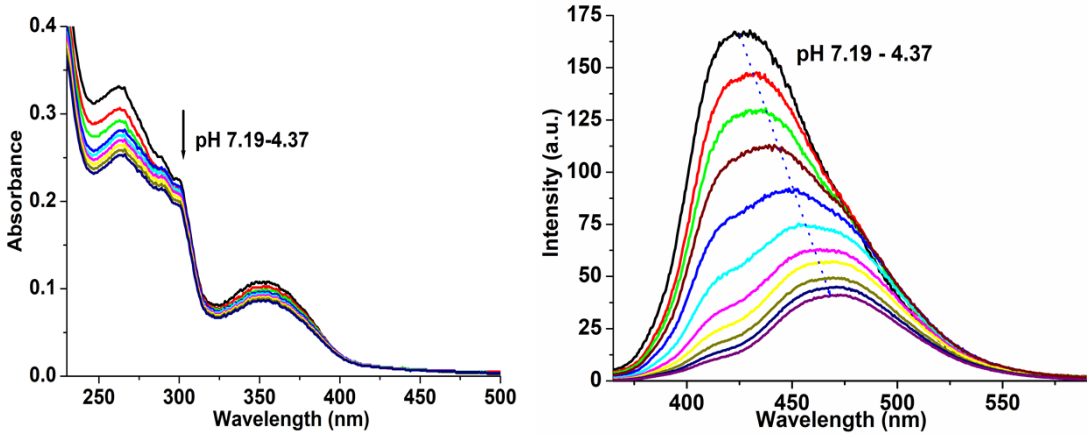

(a) (b)

Fig. S19 UV/vis (a) and Fluorescence (b) titration plot for **1** (*c*, 10 μM) with 0.1 M HCl.

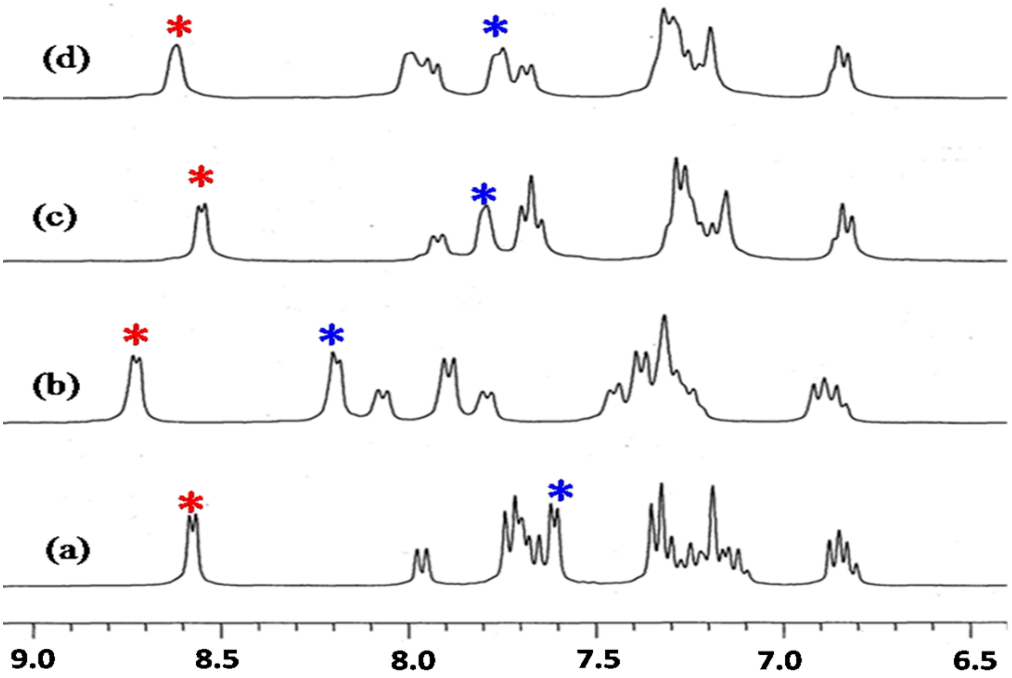

Fig. S20 ^{1}H NMR spectral titration showing the changes in absence (a) and presence of Hg^{2+} (1.0 equiv) (b), Al^{3+} (3.0 equiv) (c), and Hg^{2+} (1.0 equiv) added in the solution of **1**+Al^{3+} (3.0 equiv) (d). *H*a (red star) and *H*d protons (blue star) showing the changes in presence of Hg^{2+} (1.0 equiv) and Al^{3+} (3.0 equiv).

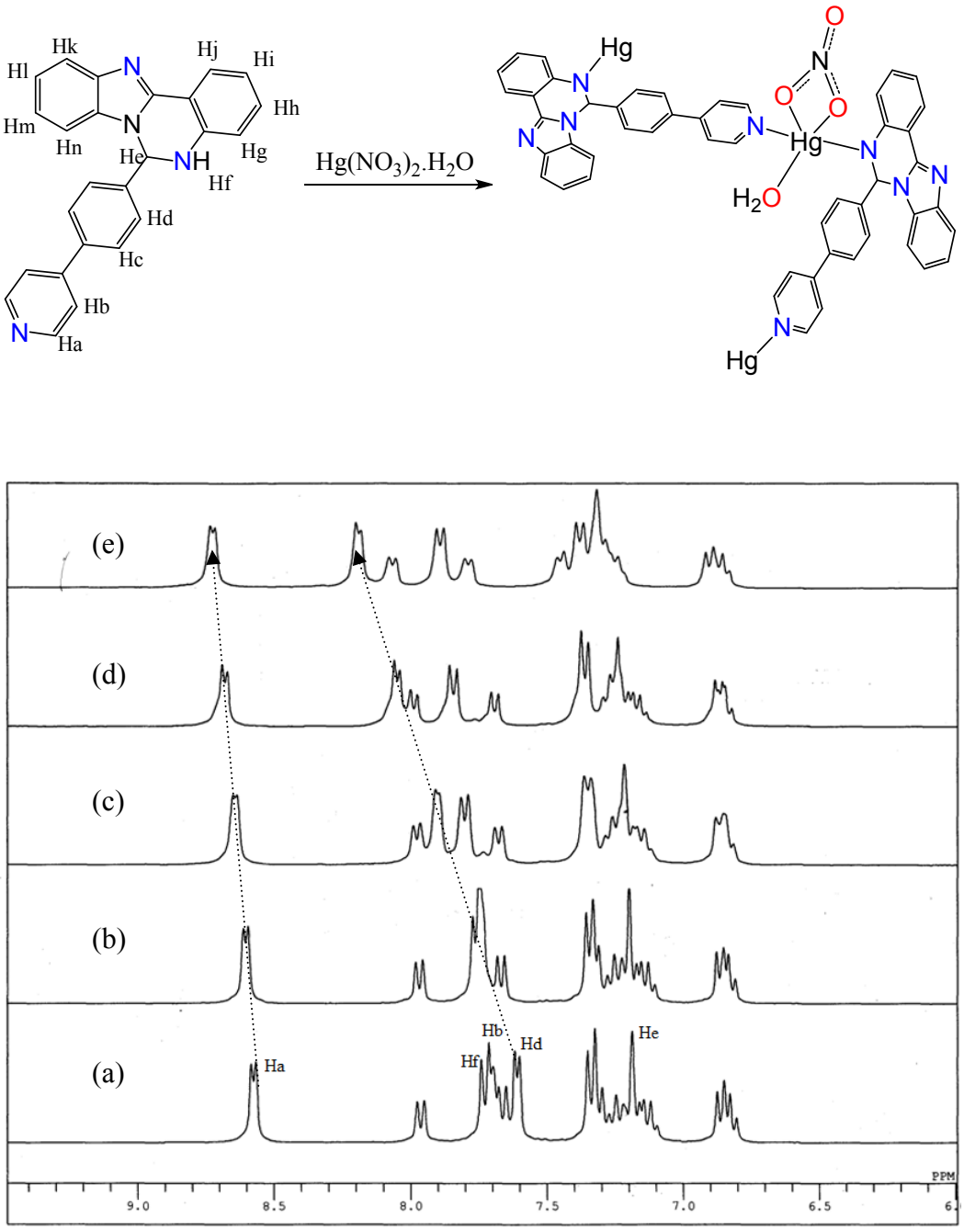

Fig. S21 ^{1}H NMR spectral titration of **1** with various amount of Hg^{2+} 0.0 equiv (a), 0.25 equiv (b), 0.50 equiv (c), 0.75 equiv (d), and 1.0 equiv (e). Arrow shows the changes mainly appeared in protons *H*a and *H*d. In the spectra proton *H*f is continually decreases and finally vanished (spectra a-e).

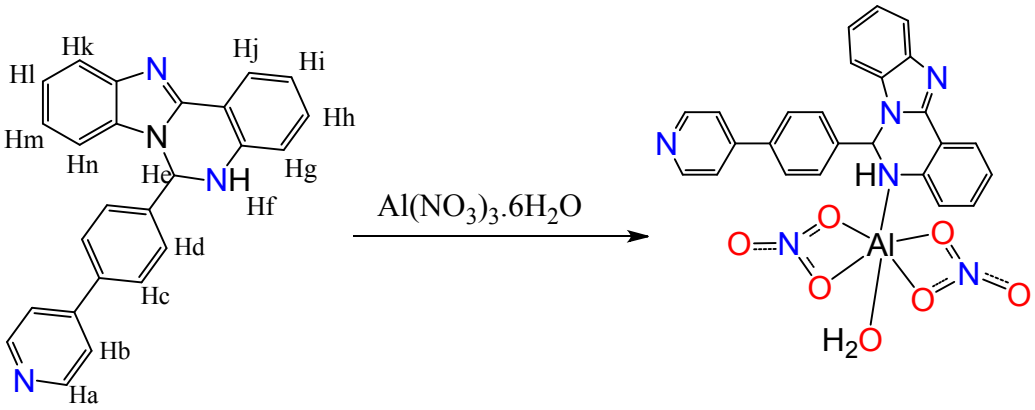

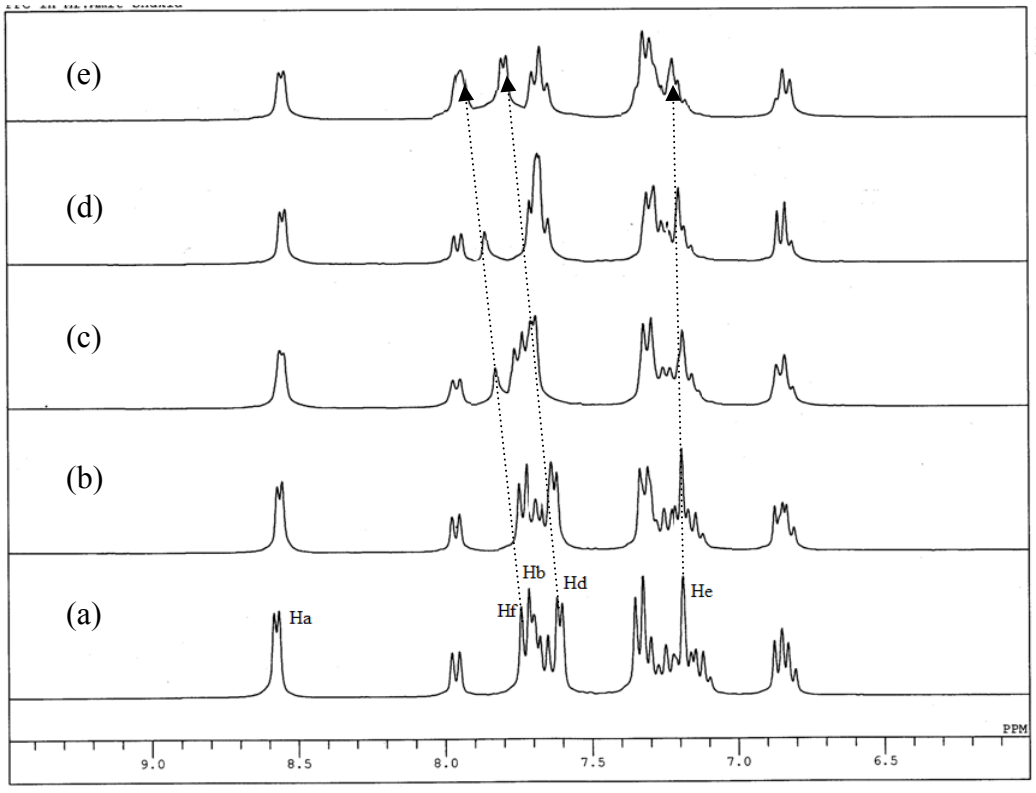

Fig. S22 ^{1}H NMR spectral titration of **1** with various amount of Al^{3+} 0.0 equiv (a), 0.50 equiv (b), 1.0 equiv (c), 2.0 equiv (d), and 3.0 equiv (e). Arrow shows the changes appeared in protons *H*d, *H*e and *H*f.

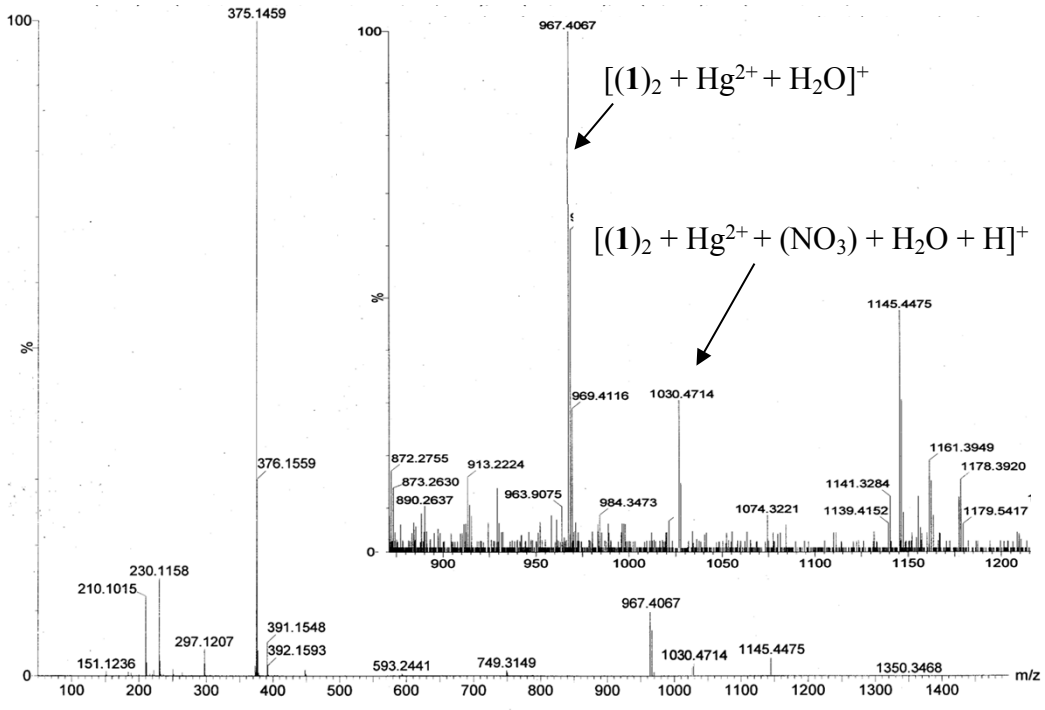

Fig. S23 ESI-MS of the (**1** + Hg^{2+}) adduct.

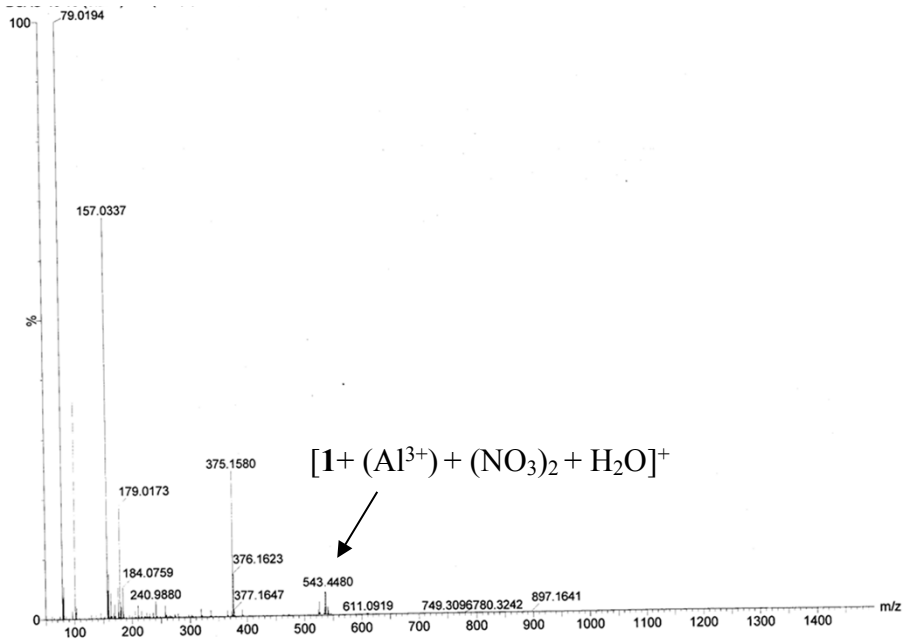

Fig. S24 ESI-MS of the (**1** + Al^{3+}) adduct.

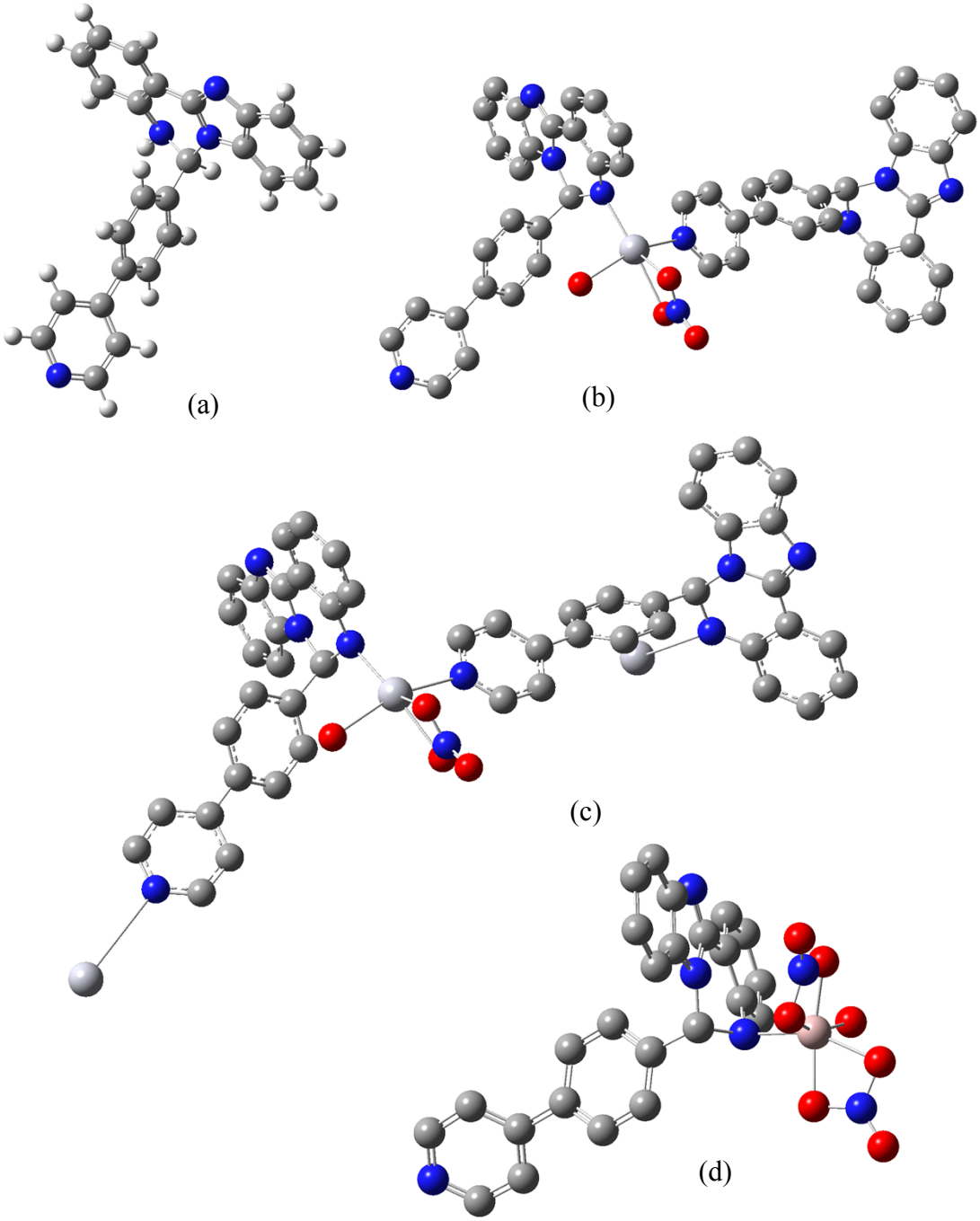

Fig. S25 Optimized structure of **1** (a), **1**+Hg^{2+} monomer unit (b), **1**+Hg^{2+} polymeric structure (c), and **1**+Al^{3+} (d).

Table S1 Comparison table for the fluorescent probes for the detection in Hg^{2+}.

Probe		Selectivity	Binding constant (M^{-1})	LOD (M)	Reference
Imidazo-quinazoline 6-(4-(pyridin-4-yl)-phenyl)-5,6-dihydrobenzo-[4,5]imidazo-[1,2-c] quinazoline **(1)**	Ratiometric Fluorescence "*turn on*"	Hg^{2+}, Al^{3+}	4.12×10^4	1.69×10^{-8}	Present manuscript
6-Ferrocenyl-5,6-dihydro[4,5]imidazo[1,2-c]-quinazoline (**4**)	Fluorescence "*turn off*"	Hg^{2+}	1.39×10^4	Not given	*Inorg. Chem*. 2012, **51**,298−311
Thiophen-2-yl-5,6-dihydrobenzo[4,5]imidazo[1,2-c]quinazo- line (**1**)	Fluorescence "*turn off*"	Hg^{2+}	0.004×10^4	2.0×10^{-7}	*Tetrahedron Lett.,* 2012, **53**, 3550-3555
Compound **QG**	Fluorescence "*turn on*"	Hg^{2+}	7.14×10^4	0.5×10^{-6}	*Chem. Commun*., 2006, 4392–4394.
Bispyrene based receptor	Fluorescence "*turn on*"	Hg^{2+}	3.38×10^{10}	7.08×10^{-6}	*Analyst*, 2010, **135**, 1600–1605
Naphthalimide substituted probe	Fluorescence "*turn on*"	Hg^{2+}	Not given	3×10^{-8}	*Chem. Eur. J.* 2012, **18**, 11188 – 11191
Tren-based rhodamine derivative	Fluorescence "*turn on*"	Hg^{2+}	1.59×10^6	Not given	*Org. Letts.*, 2007 **9**, 2501-2504
Naphthalimide-rhodamine-based dyad **1**	Ratiometric Fluorescence "*turn on*"	Hg^{2+}	Not given	Not given	*Org. Biomol. Chem.,* 2012, **10**, 8076–8081

Table S2 Comparison table for the fluorescent probes for the detection in Al^{3+}.

Probe		Selectivity	Binding constant (M^{-1})	LOD (M)	Reference
Imidazo-quinazoline 6-(4-(pyridin-4-yl)-phenyl)-5,6-dihydrobenzo-[4,5]imidazo-[1,2-c] quinazoline **(1)**	Ratiometric Fluorescence "*turn on*"	Hg^{2+}, Al^{3+}	2.45×10^3	1.44×10^{-7}	Present manuscript
Rhodamine 6G derivative (**L**)	Fluorescence "*turn on*"	Al^{3+}	3.14×10^5	3.26×10^{-6}	*Dalton Trans.,* 2014, **43**, 12624-12632
Tetrazole derivative ($\mathbf{H_2L}$)	Fluorescence "*turn on*"	Al^{3+}	1.02×10^4	5.86×10^{-6}	*Dalton Trans.,* 2014, **43**, 6429–6435
8-acetyl-7-hydroxy-4-methylcoumarin (**AHMC**)	Fluorescence "*turn on*"	Al^{3+}	-	-	*Dalton Trans.,* 2014, **43**, 2741–2743
Benzimidazole Salen ($\mathbf{H_2L}$)	Fluorescence "*turn on*"	Al^{3+}	8.08	3.3×10^{-6} (MeOH) 5.25×10^{-6} (DMSO)	*Inorg. Chem.* 2014, **53**, 3012− 3021
Schiff-base derivatives (**L**)	Fluorescence "*turn on*"	Al^{3+}	-	8.8×10^{-8}	*Org. Biomol. Chem.,* 2010, **8**, 3751–3757

References:

1 D. D. Perrin, W. L. F. Armango and D. R. Perrin, *Purification of laboratory Chemicals*, Pergamon, Oxford, UK, 1986.

2 L. J. Bartolottiand and K. Fluchick, *In Reviews in Computational Chemistry*; K. B. Lipkowitz and D. Boyd, Ed. VCH: New York, 1996, 7, 187.

3 M. J. Frisch, G. W. Trucks, H. B. Schlegel, G. E. Scuseria, M. A. Robb, J. R. Cheeseman, G. Scalmani, V. Barone, B. Mennucci, G. A. Petersson, H. Nakatsuji, M. Caricato, X. Li, H. P. Hratchian, A. F. Izmaylov, J. Bloino, G. Zheng, J. L. Sonnenberg, M. Hada, M. Ehara, K. Toyota, R. Fukuda, J. Hasegawa, M. Ishida, T. Nakajima, Y. Honda, O. Kitao, H. Nakai, T. Vreven, J. A. Jr. Montgomery, J. E. Peralta, F. Ogliaro, M. Bearpark,; J. J. Heyd, E. Brothers, K. N. Kudin, V. N. Staroverov, R. Kobayashi, J. Normand, K. Raghavachari, A. Rendell, J. C. Burant, S. S. Iyengar, J. Tomasi, M. Cossi, N. Rega, N. J. Millam, M. Klene, J. E. Knox, J. B. Cross, V. Bakken, C. Adamo, J. Jaramillo, R. Gomperts, R. E. Stratmann, O. Yazyev, A. J. Austin, R. Cammi, C. Pomelli, J. W. Ochterski, R. L. Martin, K. Morokuma, V. G. Zakrzewski, G. A. Voth, P. Salvador, J. J. Dannenberg, S. Dapprich, A. D. Daniels, Ö. Farkas, J. B. Foresman, J. V. Ortiz, J. Cioslowski and D. J. Fox, *Gaussian, Inc., Wallingford CT*, 2009.

4 (*a*) P. Hay and W. R. Wadt, *J. Chem. Phys*., 1985, **82**, 270; (*b*) W. R. Wadt and P. Hay, *J. Chem. Phys.*, 1985, **82**, 284; (*c*) P. Hay and W. R. Wadt, *J. Chem. Phys*., 1985, **82**, 299.